Red Galaxies at High Redshift

Wuyts, S.E.R.

Chapter 2

The detailed fundamental plane of two high-redshift clusters: MS 2053–04 at $z = 0.58$ and MS 1054–03 at $z = 0.83$

Abstract. We study the fundamental plane relation in high-redshift clusters using a sample of 26 galaxies in MS 2053–04 ($z = 0.583$) and 22 galaxies in MS 1054–03 ($z = 0.83$). The zero point and scatter are compared to results for lower redshift clusters in order to trace evolutionary effects. Furthermore, our large sample enables us to investigate correlations between residuals from the fundamental plane and other characteristics of the galaxies, such as color, $H\beta$ linestrength, spatial distribution, and mass. The observed scatter of the early-type galaxies with $\sigma > 100$ km s^{-1} around the fundamental plane is 0.134 and 0.106 in $\log r_e$ for MS 2053–04 and MS 1054–03 respectively. The residuals from the fundamental plane of MS 2053–04 are correlated with residuals from the $H\beta - \sigma$ relation, suggesting that stellar populations are playing a role in shaping the fundamental plane. The measured evolution in $\log M/L$ is influenced by selection effects, as galaxies with lower M/L in the Johnson B-band enter a magnitude-limited sample more easily. When we select high mass early-type galaxies to avoid this bias, we find $\log M/L_B \sim -0.47z$ and a formation redshift $z_{form} \sim 2.95$, similar to earlier results.

S. Wuyts, P. G. van Dokkum, D. D. Kelson, M. Franx & G. D. Illingworth
The Astrophysical Journal, **605**, 677 (2004)

2.1 Introduction

In the local universe early-type galaxies follow a tight scaling relation, known as the Fundamental Plane (FP). The relation between effective radius, central velocity dispersion and surface brightness $r_e \sim \sigma^\alpha I_e^\beta$, which is a plane in $(\log r_e, \log \sigma, \log I_e)$ space, was discovered by Djorgovski & Davis (1987) and Dressler et al. (1987). In combination with the virial theorem

$$M/L \sim \sigma^2 r^{-1} I_e^{-1} \tag{2.1}$$

the small scatter around the FP implies that, under the assumption of homology, the M/L ratios of early-type galaxies are well behaved and scale as

$$M/L \sim \sigma^{\alpha/\beta+2} r_e^{-(1+\beta)/\beta}. \tag{2.2}$$

As the M/L ratio increases with ageing of a stellar population, the FP is a useful tool in research on galaxy formation and evolution. Based on a sample of 226 E and S0 galaxies in 10 clusters of galaxies, Jørgensen, Franx,& Kjærgaard (1996, hereafter JFK96) concluded the local plane in the Johnson B band has the form:

$$\log r_e = 1.20 \log \sigma - 0.83 \log I_e + \gamma \tag{2.3}$$

which implies that

$$M/L \sim M^{0.28} r_e^{-0.07}. \tag{2.4}$$

Later studies on intermediate and high-redshift clusters of galaxies used the zero-point shift of the plane to estimate average formation redshifts of the stars in early-type galaxies (e.g., Bender et al. 1998; van Dokkum et al. 1998, hereafter vD98; Jørgensen et al. 1999; Kelson et al. 2000c, hereafter K2000; Pahre et al. 2001; van Dokkum & Stanford 2003). The scatter around the plane provides constraints on the spread in galaxy ages.

The slope of the FP (and other scaling relations) constrains systematic age trends with mass and other parameters. Any evolution of the slope of the FP with redshift implies that the ages of the stellar populations are correlated with galaxy mass. For the cluster CL1358+62 at z = 0.33 K2000 finds that the slope of the FP has not evolved significantly over the past $\sim$ 4 Gyr. The sample of 5 bright MS 2053–04 galaxies used by Kelson et al. (1997, hereafter K97) to study the FP at z = 0.583 seemed to agree with the values of coefficients α and β as given by JFK96. However, the sample was too small to perform a proper fit. The same conclusions were drawn for MS 1054–03 at z = 0.83 based on 6 early-type galaxies (vD98). In this chapter, we investigate the FP of MS 2053–04 and MS 1054–03 early-type galaxies using larger samples spread over a larger range of distances from the brightest cluster galaxies (BCG). In §2.2 we discuss the spectroscopy, sample selection and velocity dispersions. Imaging and measurement of the structural parameters is described in §2.3. Zero point of the FP with JFK96 coefficients and scatter around the plane are discussed in §2.4. In §2.5 we study correlations between the residuals from the FP and various other properties of the galaxies. Finally the conclusions are summarized in §2.7. Vega magnitudes are used throughout this chapter. We use $H_0 = 70$ km s^{-1} Mpc^{-1}, $\Omega_\Lambda = 0.7$, and $\Omega_M = 0.3$, but note that our results are independent of the value of the Hubble constant.

2.2 Spectroscopy

2.2.1 Sample selection and observations

All spectra used in the FP analysis were obtained with the LRIS spectrograph (Oke et al. 1995) on the 10 m W.M. Keck Telescope. The data were obtained in a series of observing runs from 1996 to 2002. The majority of galaxies in our final sample were selected on the basis of their spectroscopic redshift and their I- or F814W-band magnitude. The samples were limited at $I \approx 22$ for all runs; galaxies with $I \lesssim 21$ were given highest priority in the mask designs. The redshift information came from a large I-selected spectroscopic survey of both clusters described in detail in Tran et al. (1999), van Dokkum et al. (2000), and Tran (2002). For the initial MS 1054–03 observing runs only limited redshift information was available, and we applied color criteria to select likely cluster members. Galaxies having $\Delta(R-I) - 0.25\Delta(B-R) < -0.4$, with $\Delta(R-I)$ and $\Delta(B-R)$ colors relative to the central galaxy, were excluded. The color ranges were chosen such that blue cluster members were unlikely to be excluded. The final FP sample of MS 1054–03 contains 19 galaxies that were selected with these mild color constraints. No morphological information was used in the selection process.

For most observations we used the 600 lines mm^{-1} grating blazed at 7500 Å; some of our earlier data were taken with the 831 lines mm^{-1} grating blazed at 8200 Å (see vD98). The wavelength coverage was typically ~ 3500 to ~ 5400 Å in the rest frame. Exposure times ranged from 7500 s to 33400 s and from 10500 s to 22800 s for the MS 2053–04 and MS 1054–03 galaxies respectively. The instrumental resolution was typically $\sigma_{inst} \sim 40 - 80$ km s^{-1} and signal-to-noise ratios ranged from 20 to 100 $\mathrm{Å}^{-1}$ in the observed-frame (in the continuum).

A total of 43 galaxies (26 early-type) were observed in MS 2053–04. The MS 1054–03 sample contained 30 galaxies (14 early-type). The morphological classification is described in §2.3.3. Early-type galaxies include E, E/S0 and S0 morphologies.

2.2.2 Basic reduction

The spectra were reduced using our own software and standard IRAF software routines (see, e.g., Kelson et al. 2000b). The wavelength calibration was performed using the night sky emission lines. The typical rms scatter about the fitted dispersion solutions is about 1/15 of a pixel. Since the dispersion is about 1.28 Å pixel^{-1} for the data taken with the 600 mm^{-1} grating (and 0.92 Å pixel^{-1} for the 831 mm^{-1} data), the rms scatter is equivalent to velocity errors smaller than 5 km s^{-1}.

The flat-fielding accuracy is generally better than a percent, on small scales. The data have not been accurately flux-calibrated so on large scales, the notion of flat-fielding accuracy is not meaningful. There tend to be moderate-scale (k=100 $\mathrm{Å}^{-1}$) residuals in the flat-fielding that are the result of a mismatch between the fringing in the flat-fields and the fringing in the data. Such inaccuracies in de-fringing the data have no effect on the velocity dispersions because the spectra are effectively filtered on those scales (and larger) in the process of matching the continua of the template and galaxy spectra.

The subtraction of the sky was performed using standard, published, and well-tested methods: for each galaxy the two-dimensional spectra were first rectified, and

then 1st- or 2nd-order polynomials were fit to the pixels on both sides of the galaxy, typically excluding the few arcsec where the galaxy is bright. An iterative clipping routine was used to reject any remaining bad pixels from the fit, similar to what IRAF allows the user to do. These methods have been discussed elsewhere at great length and we choose not to bore the reader with very familiar territory. While more complicated and precise means of sky subtraction are now available (see Kelson 2003), these data were analyzed before such methods became available, and the accuracy of the sky subtraction performed in the "traditional" way is satisfactory for our purposes.

The slit widths varied slightly with each run, ranging from $0\farcs90$ to $1\farcs05$. The extraction apertures for MS 2053–04 and MS 1054–03 were 7 CCD rows (or $1\farcs5$).

2.2.3 Velocity dispersions

Velocity dispersions were measured with a direct fitting method (Kelson et al. 2000b). Details of the fitting procedure are given in Kelson et al. (2006). Direct fitting methods provide several advantages over Fourier-based techniques. Most importantly, pixels are no longer weighted uniformly in the computation of the fitting metric (in this case χ^2). As in Kelson et al. 2000b, we weight each pixel by the inverse of the expected noise (photon and electronic read noise). Furthermore, the spectra that exhibit strong Balmer absorption had those features given zero weight in the fitting, in order to minimize the contribution of those features to template mismatch error, and also to ensure that our estimates of σ reflected the old, underlying stellar populations. We typically fit the spectra over a ~ 1000 Å wavelength range (in the rest frame). We used a range of template stars, from G5 through K3 and adopted the template star that gave the lowest mean χ^2. In both clusters, HD102494, a G9IV star, was the "best" template.

Both observations and simulations by Jørgensen et al. (1995b) showed that, at low S/N, measured velocity dispersions were systematically too large. At the same S/N, this systematic effect was largest for the galaxies with velocity dispersions below 100 km s^{-1}. Therefore, we omit all galaxies with $\sigma < 100$ km s^{-1} from our samples. Furthermore, we limit our samples to sources with an error in σ smaller than 15 %. Errors in the dispersion and velocity are initially determined from the local topology of the $\chi^2(\sigma, V)$ surface.

Seven MS 2053–04 galaxies with $\sigma > 100$ km s^{-1} were observed both during the 1997 and 2001 observing run. A direct comparison between the derived velocity dispersions (prior to the aperture correction) is presented in Figure 2.1. Generally, the agreement is good, with one outlier. All spectra have similar S/N. The rms value of $\frac{\sigma_{97}-\sigma_{01}}{\sqrt{d\sigma_{97}^2+d\sigma_{01}^2}}$ is 1.23, slightly higher than the expected value of 1. The mean deviation between the two runs is $-2 \pm 5\%$, consistent with zero. We conclude there is no evidence for systematic effects and conservatively multiply all errors by the factor 1.23.

The final sample consists of 26 galaxies (19 early-type) in MS 2053–04 and 22 galaxies (12 early-type) in MS 1054–03. We applied an aperture correction to a nominal aperture of $D = 3\farcs4$ at the distance of Coma (see JFK96). The final velocity dispersions have therefore been multiplied by a factor of 1.057 for MS 2053–04 and 1.062 for MS 1054–03. This correction allows for a fair comparison between clusters at a range of redshifts. The data are tabulated in Table 2.1.

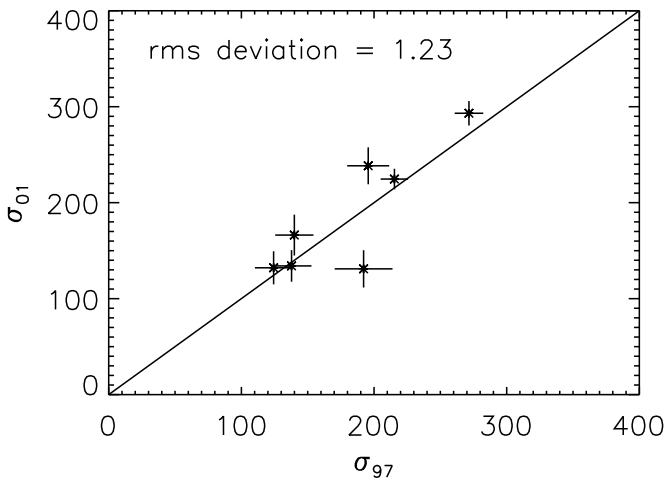

Figure 2.1 — A direct comparison of velocity dispersions for 7 galaxies in MS 2053–04. Measured σ values, prior to aperture correction, for the 2001 run are plotted against σ values from the 1997 spectra. Formal errors derived from $\chi^2(\sigma, V)$ are drawn. Based on this overlap sample, actual error bars are estimated to be 23% larger.

2.3 Imaging

For both MS 2053–04 and MS 1054–03 large HST WFPC2 mosaics were obtained, each consisting of 6 pointings. Both clusters were observed in the F606W and F814W filters. The layout of the MS 2053–04 mosaic is described in Hoekstra et al. (2002). Exposure times were 3300 s in F606W and 3200 s in F814W per pointing. The MS 1054–03 mosaic is described in van Dokkum et al. (2000); exposure times were 6500 s for each pointing and in each filter. Interlacing of the images improved the sampling by a factor $\sqrt{2}$ for MS 1054–03.

2.3.1 Structural parameters

In this section, we describe the measurement of effective radii r_e and surface brightnesses at those radii I_e. For the Johnson B passband, I_e in $L_\odot$ pc^{-2} is related to μ_e in mag arcsec^{-2} as

$$\log I_e = -0.4(\mu_e - 27.0). \tag{2.5}$$

We created postage stamps sized $12\farcs8 \times 12\farcs8$ for the 26 MS 2053–04 and 22 MS 1054–03 galaxies and fit 2D $r^{1/n}(n = 1, 2, 3, 4)$ law profiles, convolved with Point Spread Functions (PSF), to the galaxy images. As PSFs depend on the positions of objects on the CCDs, we used Tiny Tim v6.0 to create an appropriate PSF for each galaxy. Other parameters determining the shape of the PSF are template spectrum (M type star), PSF size (3″), sampling and filter (F814W). The code allows simultaneous fitting of the object of interest and any neighbouring objects. The fits were restricted to radii of 3″ to 5″ around the objects, depending on their size. Image defects were masked in the fit, as well as neighbouring galaxies not well fitted by $r^{1/4}$ laws. All other pixels got uniform weight.

We performed the $r^{1/n}$ fits for Sersic numbers n = 1 (exponential), 2, 3 and 4 (de Vaucouleurs law). In this chapter, we always use r_e and I_e based on $r^{1/4}$ fits to all galaxies on the postage stamps, even if other Sersic numbers result in a better χ^2 of the fit. Fitting a $r^{1/4}$ profile resulted in a $\chi^2 < 1.5$ for 69% of all galaxies; 86% have $\chi^2 < 2$.

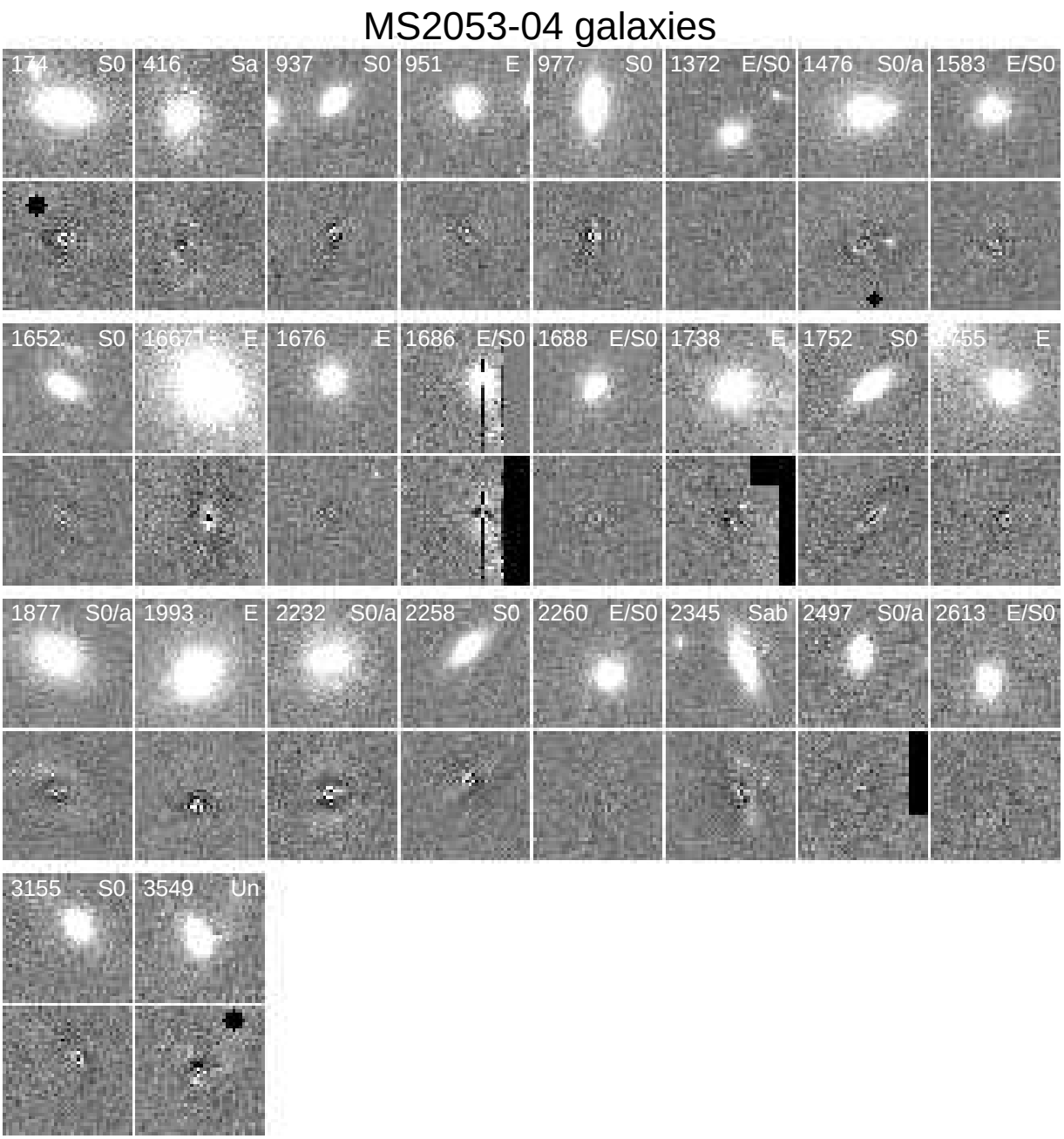

Figure 2.2 — $4'' \times 4''$ images (*upper*) and residuals (*lower*) after $r^{1/4}$ profile fitting for the galaxies in MS 2053–04. Masked regions are indicated in black. The postage stamps prove that our results for the early-type galaxies are not suffering from misclassifications or bad profile fitting.

The galaxies in our final samples together with the residuals after profile fitting are presented in Figure 2.2 (MS 2053–04) and Figure 2.3(MS 1054–03).

2.3.2 Error in the structural parameters

For MS 1054–03 each of the 6 pointings was observed twice, with a shift of 0.5 pixels, providing a direct way to measure the error in the structural parameters. From fits

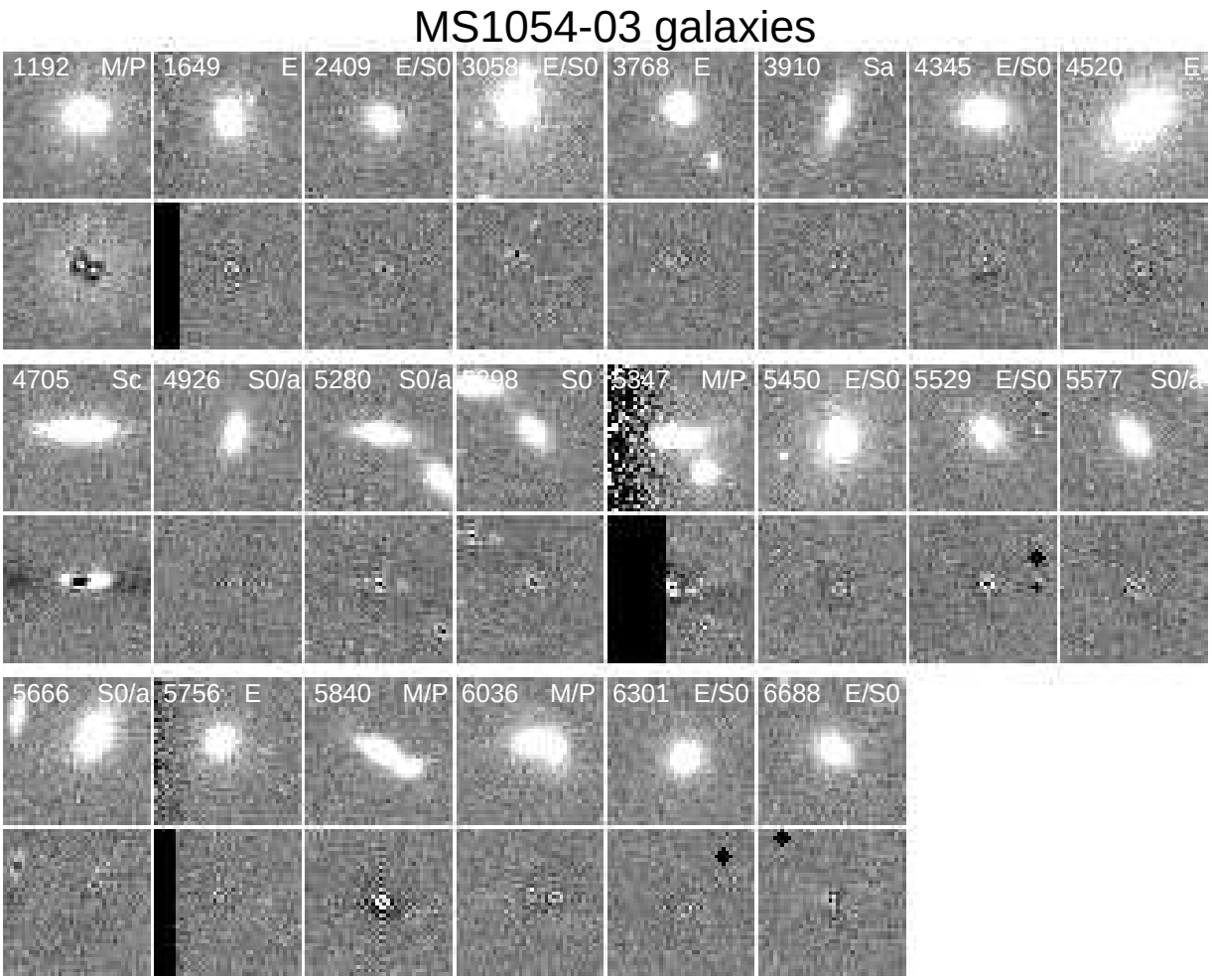

Figure 2.3 — $4'' \times 4''$ images (*upper*) and residuals (*lower*) after $r^{1/4}$ profile fitting for the galaxies in MS 1054–03. Masked regions are indicated in black. The postage stamps prove that our results for the early-type galaxies are not suffering from misclassifications or bad profile fitting.

to the two independent observations we infer that errors are small ($< 4\%$ in r_e) for galaxies larger than $0\farcs83$. The error in r_e rises to at most 18.5% for smaller sources. Though this might seem problematic, we note that this large error does not enter the FP analysis as the combination $r_e I_e^{-\beta}$ enters the FP. Using $\beta = -0.83$ from JFK96, the error in the FP parameter $r_e I_e^{0.83}$ is limited to $\sim 2.1\%$ rms, ignoring one outlier with 30% offset. The fit of a de Vaucouleurs profile to the outlier ID5347 with merger/peculiar morphology is clearly unstable. The uncertainty in the FP parameter is comparable to the $\sim 2.5\%$ rms error estimate from Kelson et al. (2000a). The small error in the FP parameter is an artifact of the slope of the de Vaucouleurs growth curve. Hereafter, we use the average of the independent r_e measurements (which reduces the error by $1/\sqrt{2}$) and the I_e corresponding to this average value, using the empirical result that $r_e I_e^{0.66}$ is the most stable combination of the structural parameters. In general we can conclude from the error analysis that random errors are small. Therefore the scatter found around the FP will not be due to errors in the photometry.

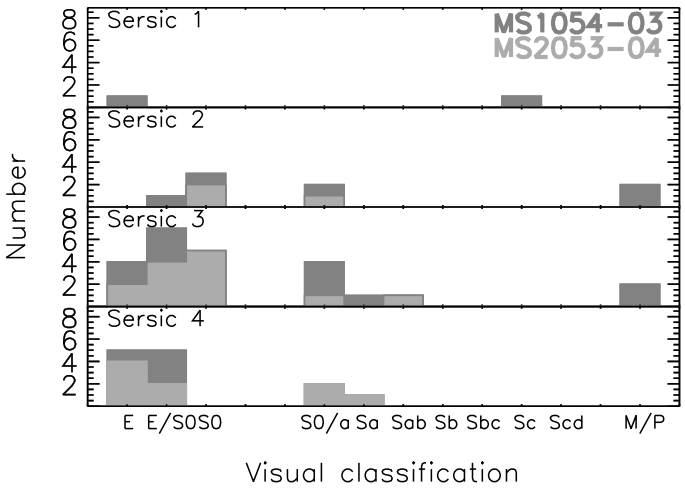

Figure 2.4 — Visual classification histogram for different best fitting Sersic numbers. Early-type morphologies generally correspond to Sersic numbers 3 and 4. A different greyscale is used for MS 2053–04 and MS 1054–03.

2.3.3 Visual and quantitative classifications

Galaxies were visually classified by P. G. van Dokkum, M. Franx,& D. Fabricant using the procedure as described in Fabricant, Franx,& van Dokkum (2000). In this chapter, we consider cluster members with early-type morphology (E, E/S0, S0). Late-type morphologies are also plotted, but are not included in fitting procedures unless we mention otherwise. A quantitative alternative to the classification by eye is based on the Sersic number that results in the smallest χ^2 of the profile fit.

Figure 2.4 shows histograms of the visual classifications for the galaxies with best fitting Sersic number 1, 2, 3 and 4. As could be expected, early-type morphologies generally correspond to Sersic numbers 3 and 4. We note that the difference in χ^2 between n = 3 and 4 is often too small to consider them as a separate class of objects. We conclude that the visual and quantitative classifications divide the sample in roughly the same bulge and disk dominated classes.

2.3.4 Transformation to rest-frame magnitude

In order to compare the FP of MS 2053–04 and MS 1054–03 with the FP of Coma at $z = 0.023$, we have to transform the effective radius to units of kpc. Furthermore, for a meaningful comparison it is necessary to study all data in a common photometric band in the rest frame of the galaxies. The observed F606W and F814W filters straddle the redshifted B_z band for $0.5 \leq z \leq 0.8$. Therefore, we transform the observed surface brightnesses to rest-frame B. The procedure is described in van Dokkum & Franx (1996). It involves an interpolation between F606W and F814W, and is different from applying a "K-correction". For $z = 0.583$ we find

$$\mu_{B_z} = \mu_{F814W} + 0.42(F606W - F814W) + 0.84, \tag{2.6}$$

and for $z = 0.83$

$$\mu_{B_z} = \mu_{F814W} + 0.01(F606W - F814W) + 1.13. \tag{2.7}$$

Table 2.1. FP sample

MS 2053–04								MS 1054–03							
ID	$\Delta R.A.$[a] [″]	ΔDec[a] [″]	$\log r_e$ [kpc]	μ_{B_z}[b] [mag ″$^{-2}$]	σ [km s^{-1}]	$F814W^T$ [mag]	Type	ID	$\Delta R.A.$[c] [″]	ΔDec[c] [″]	$\log r_e$ [kpc]	μ_{B_z}[b] [mag ″$^{-2}$]	σ [km s^{-1}]	$F814W^T$ [mag]	Type
174	9.34	-206.60	0.588	21.19	225 ± 13	19.68	S0	1192	136.10	-58.31	0.518	20.51	138 ± 15	20.24	M/P
416	29.26	-150.90	0.833	22.92	144 ± 14	20.48	Sa	1649	122.30	-16.89	0.565	20.80	243 ± 28	20.69	E
937	-30.58	-119.80	-0.223	18.20	127 ± 11	20.70	S0	2409	84.18	-24.01	0.574	21.26	287 ± 33	21.36	E/S0
951	-31.74	-118.00	0.288	20.88	151 ± 13	20.81	E	3058	52.73	-9.72	1.227	22.97	303 ± 33	19.83	E/S0
977	-72.15	-132.10	0.261	19.92	249 ± 11	20.03	S0	3768	38.86	-0.38	0.507	20.78	222 ± 24	21.04	E
1372	-39.50	-72.32	0.153	20.88	164 ± 14	21.55	E/S0	3910	32.00	-11.84	0.457	20.67	295 ± 42	21.23	Sa
1476	-38.26	-54.80	0.505	21.33	143 ± 16	20.04	S0/a	4345	21.51	-13.22	0.643	20.98	336 ± 34	20.55	E/S0
1583	-24.76	-41.87	0.289	21.04	143 ± 10	21.04	E/S0	4520	0	0	1.141	22.29	322 ± 30	19.48	E
1652	-9.65	-27.37	0.475	21.94	181 ± 13	21.12	S0	4705	6.10	8.34	1.006	22.22	253 ± 36	20.61	Sc
1667	0	0	1.103	22.65	292 ± 10	18.56	E	4926	-4.07	-3.68	0.387	20.43	310 ± 38	21.32	S0/a
1676	47.76	0.89	0.415	21.56	125 ± 14	20.76	E	5280	-20.46	20.82	0.548	21.06	259 ± 31	21.17	S0/a
1686	14.28	-12.29	0.408	21.58	129 ± 15	20.95	E/S0	5298	-21.74	19.24	0.550	21.38	284 ± 39	21.52	S0
1688	-9.00	-22.49	0.392	21.78	138 ± 13	21.31	E/S0	5347	-34.24	56.37	0.795	21.54	254 ± 24	20.58	M/P
1738	-23.00	-17.84	0.667	22.04	124 ± 13	20.01	E	5450	-46.30	-3.51	0.866	21.72	234 ± 26	19.98	E/S0
1752	-1.54	-9.86	0.353	21.08	151 ± 17	20.88	S0	5529	-37.79	31.29	0.549	20.99	182 ± 23	21.01	E/S0
1755	-1.14	-3.41	0.482	21.48	234 ± 23	20.23	E	5577	-43.54	48.16	0.501	20.75	305 ± 40	21.05	S0/a
1877	19.96	15.62	0.683	22.07	169 ± 14	20.17	S0/a	5666	-58.07	-83.77	0.731	21.20	286 ± 23	20.50	S0/a
1993	49.67	43.54	0.540	20.86	212 ± 8	19.40	E	5756	-59.26	97.86	0.551	20.91	232 ± 27	20.93	E
2232	-82.50	13.16	0.664	22.01	141 ± 12	20.16	S0/a	5840	-52.17	23.03	0.090	18.38	212 ± 26	20.66	M/P
2258	-2.50	45.70	0.264	20.77	134 ± 18	20.93	S0	6036	-63.37	-29.09	0.559	21.17	254 ± 22	21.18	M/P
2260	46.61	67.51	0.490	21.80	140 ± 14	20.81	E/S0	6301	-70.57	25.38	0.565	21.03	249 ± 24	20.99	E/S0
2345	16.82	67.38	0.601	21.99	152 ± 19	20.58	Sab	6688	-91.54	-41.79	0.458	20.50	274 ± 37	20.82	E/S0
2497	15.46	78.88	0.451	21.71	244 ± 14	21.13	S0/a								
2613	-23.80	71.80	0.584	22.39	171 ± 25	21.07	E/S0								
3155	-90.37	98.46	0.376	21.09	203 ± 18	20.64	S0								
3549	-29.45	165.70	0.307	20.70	155 ± 19	20.45	Un								

[a]Coordinates with respect to the BCG of MS 2053–04: ID1667 at (20:56:21.4; -04:37:50.8) (J2000).

[b]Surface brightnesses μ_{B_z} are corrected for galactic extinction and cosmological dimming.

[c]Coordinates with respect to the BCG of MS 1054–03: ID4520 at (10:56:59.9; -03:37:37.3) (J2000).

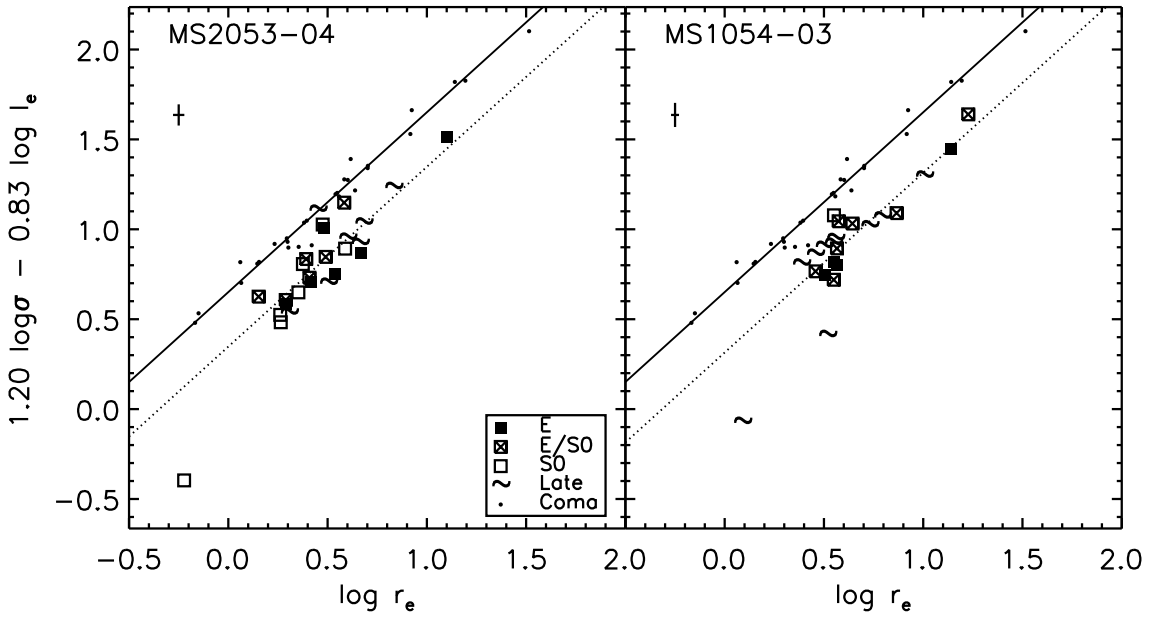

Figure 2.5 — The fundamental plane of clusters MS 2053–04 (z=0.583) and MS 1054–03 (z=0.83). The Coma FP is drawn for reference. Typical error bars are plotted in the upper left corner. Cluster galaxies in the higher redshift clusters follow the FP scaling relation, but with an offset with respect to Coma. Galaxies with early-type morphologies show a larger scatter than in the local universe.

The $F606W - F814W$ colors in (2.6) and (2.7) are obtained using SExtractor (Bertin & Arnouts 1996) with fixed apertures of $0\farcs7$ diameter. Extinction corrections for both fixed aperture colors and surface brightnesses were derived from Schlegel et al. (1998). Another correction compensates for cosmological dimming $\propto (1+z)^4$. The final samples are summarized in Table 2.1. Included are the coordinates with respect to the BCG, aperture corrected σ, r_e, μ_{B_z} corrected for galactic extinction and cosmological dimming, total $F814W^T$ magnitudes and morphological classifications.

2.4 The fundamental plane

In this section we discuss the FP relation in MS 2053–04 and MS 1054–03. For determination of the zero point and scatter we adopt the slope $(\alpha, \beta) = (1.20, -0.83)$ that JFK96 found for the local B-band FP. In Figure 2.5 we show the edge-on view of the FP for both clusters. Different symbols indicate different morphological types. For comparison the Coma FP is drawn as well. The galaxies in MS 2053–04 and MS 1054–03 follow a similar FP, but with an offset with respect to Coma.

2.4.1 Zero point and scatter

2.4.1.1 MS 2053–04

Using the biweight mean (Beers et al. 1990) we fit a zero point of the FP to the early-type galaxies in MS 2053–04. Under the assumption of homology, the zero-point shift of the FP traces the mean evolution of the galaxy M/L ratio. The observed zero-point off-

Table 2.2. MS 2053–04 and MS 1054–03 zero point and scatter around FP. Earlier results from K97 and vD98 are also in this Table.

Sample	# objects	$\Delta\log(M/L_B)$ (biweight mean)	$\Delta\log(M/L_B)$ (median)	Scatter in $\log r_e$ (biweight)
MS 2053–04 early-type	19	-0.365 ± 0.037	-0.404 ± 0.037	0.134 ± 0.034
MS 2053–04 Sersic34	23	-0.382 ± 0.028	-0.404 ± 0.028	0.111 ± 0.024
MS 2053–04 K97	5	-0.280 ± 0.036	-0.257 ± 0.036	0.058 ± 0.018
MS 1054–03 early-type	12	-0.405 ± 0.037	-0.418 ± 0.037	0.106 ± 0.023
MS 1054–03 Sersic34	15	-0.368 ± 0.027	-0.392 ± 0.027	0.086 ± 0.026
MS 1054–03 vD98	6	-0.393 ± 0.040	-0.405 ± 0.040	0.049 ± 0.018

set is $\Delta\log(M/L_B) = -0.365 \pm 0.037$, larger than $\Delta\log(M/L_B) = -0.280 \pm 0.036$ found by K97 based on older data for a sample of 5 bright galaxies. We will return to this issue in §2.5.

We find a biweight scatter for the early-type population in MS 2053–04 as large as 0.134 ± 0.034 in $\log r_e$, with the error derived from bootstrapping. This is significantly larger than the observed scatter of 0.071 around the B-band FP of local clusters (JFK96). After subtraction of the measurement uncertainties in quadrature, we find the intrinsic scatter for the early-type galaxies to be 0.124 ± 0.037. We conclude that measurement uncertainties cannot account for all of the enhanced scatter. Not only is the scatter larger than in the local universe, it also exceeds the previous result of 0.058 ± 0.018 obtained by K97. Our new measurements for 4 early-type galaxies that were also in the K97 sample give a scatter of 0.116 ± 0.035 (as opposed to 0.050 ± 0.018 for the original K97 data on these 4 galaxies). A larger sample and new data on previously studied objects leads to the conclusion that the early-type galaxies in MS 2053–04 show a considerably larger spread around the FP than early-type galaxies in the local universe.

We next analyzed the scatter of the bulge-dominated systems selected by Sersic index (3 and 4), which is a more objective method of classifying. The scatter drops by about 20% with respect to the classification by eye, to 0.111 ± 0.024. Using both visual and quantitative classifications, we find that bulge-dominated systems in MS 2053–04 are less tightly confined to a plane than in the local universe by a factor 1.5 to 2.

Zero-point shifts and scatters from biweight statistics are summarized in Table 2.2. Median zero-point shifts are given for comparison.

2.4.1.2 MS 1054–03

For the early-type galaxies in MS 1054–03 the zero-point offset agrees well with the previous result from vD98 [$\Delta\log(M/L_B) = -0.405 \pm 0.037$ for the new sample and $\Delta\log(M/L_B) = -0.393 \pm 0.040$ from vD98]. The observed scatter is 0.106 ± 0.024, and the intrinsic scatter is 0.086 ± 0.028, consistent with the scatter in local clusters (JFK96). Using new measurements of 5 MS 1054–03 early-type galaxies studied by vD98, we obtain a biweight scatter of 0.062 ± 0.018, consistent with 0.047 ± 0.024 for the original vD98 data on these objects. As for MS 2053–04, the scatter decreases by roughly 20% if we select bulge-dominated systems by Sersic index (3 and 4) instead of by eye.

2.5 Correlations with other parameters

One of the striking effects we found in §2.4.1 is the large FP scatter for MS 2053–04. Here we investigate the cause of this enhanced scatter. In the case of a stellar population effect such as variations in age, metallicities or dust content, we expect the residual from the FP to correlate with color and linestrength indices. We also discuss the residual from the FP as a function of environment and investigate the dependence on galaxy mass. Hereafter, we again adopt the JFK96 slope and we express residuals from the FP as deviations in $\log(M/L_B)$. A positive residual means the galaxy has a higher M/L than the FP prediction based on its r_e and σ. The approach of measuring offsets along the surface brightness axis is physically intuitive since -if we ignore mergers- a galaxy only moves along this axis during its lifetime. For consistency with our FP analysis, we adopt locally determined slopes for all other considered scaling relations as well. In Figure 2.6 the residual from the FP is plotted against various properties for both clusters. Different symbols refer to different morphological classes. For each panel, the probability that a random sample has the same Spearman rank order correlation coefficient as the early-type galaxies in our sample, is printed in the corner.

2.5.1 The color-magnitude relation

The most straightforward interpretation for the large scatter is a stellar population effect. For age, metallicity, and dust trends, we expect lower M/L ratios than the FP prediction to correlate with bluer colors than the CMR prediction. We refer the reader to Tran et al. (2003) for the color-magnitude relation of MS 2053–04 and to van Dokkum et al. (2000) for the MS 1054–03 CMR. Similar to our FP analysis, we assume that the slope of the relation does not evolve and adopt the slope measured in the Coma cluster by Bower, Lucey,& Ellis (1992b). After conversion of the (F606W,F814W) photometry to Johnson U and V (using the same procedure as K2000), we fit a CMR zero point to the early-type galaxies in our samples. A positive residual ΔCMR in Figure 2.6(a) and Figure 2.6(b) corresponds to a redder color of the galaxy than the CMR prediction based on its total V magnitude. The Spearman rank order correlation coefficient points in the expected direction for a stellar population effect. However, the level of significance is insufficient to confirm that galaxies with lower M/L than the FP prediction are bluer and the higher (more evolved) ones are redder than the CMR prediction.

2.5.2 $H\beta$ linestrength

Apart from M/L ratio (residual from FP) and color (residual from CMR), strengths of absorption lines are a valuable tool for tracing stellar population effects. In this section we discuss the $H\beta$ index (expressed in Å, see Trager et al. 1998). $H\beta$ is an age-sensitive parameter with only a minor contribution due to metallicity. For spectral reduction and derivation of linestrengths we refer the reader to Kelson et al. (2006).

The $H\beta - \sigma$ relation for early-type galaxies in the Coma cluster was derived from the $H\beta_G - \sigma$ relation presented by Jørgensen (1999). The $H\beta_G$ index is related to the Lick/IDS $H\beta$ index as $H\beta_G = 0.866 H\beta + 0.485$ (Jørgensen 1997). Assuming a non-evolving slope of the $H\beta - \sigma$ scaling relation, we fit a zero point to the relation in MS 2053–04 and MS 1054–03.

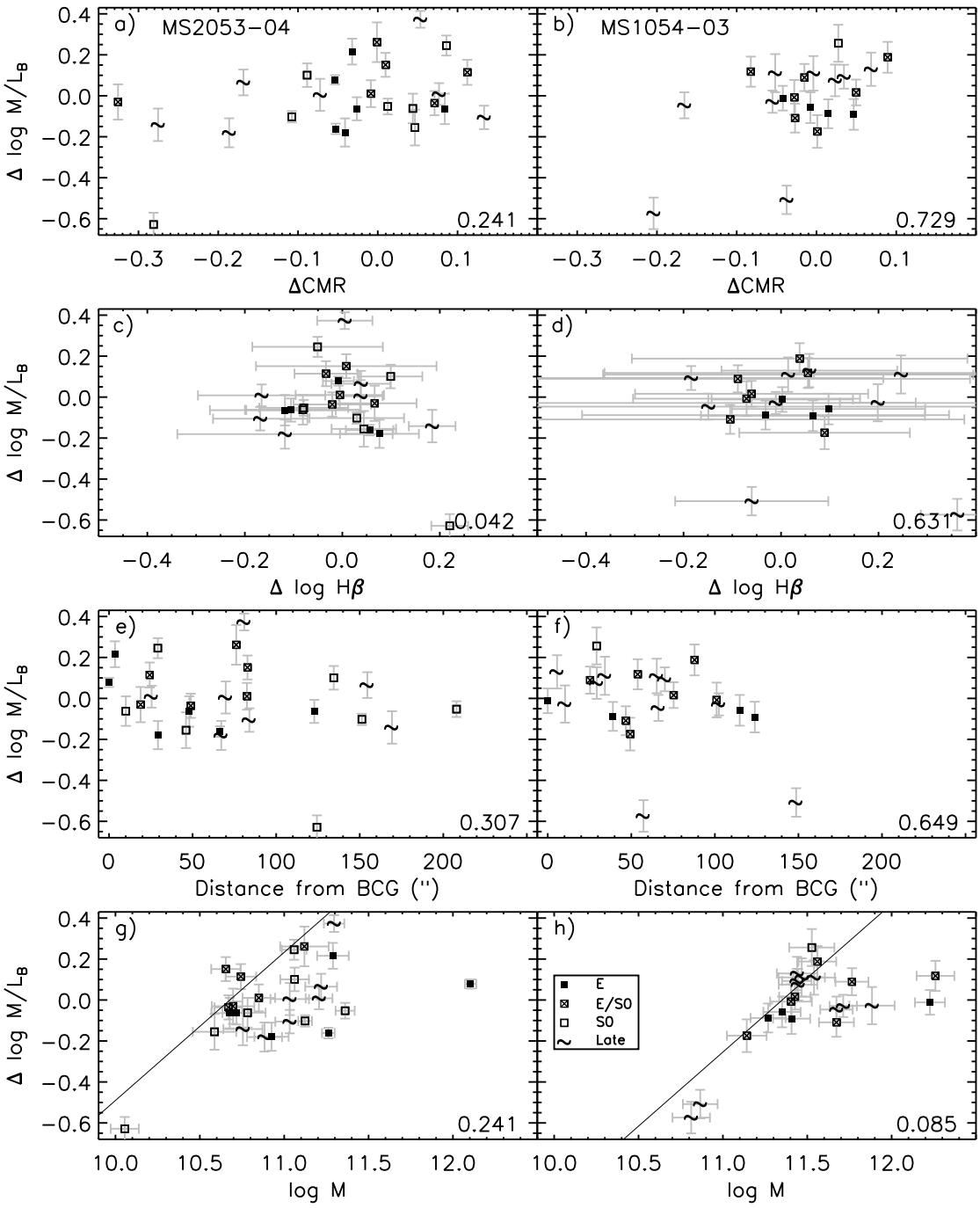

Figure 2.6 — Residual from the fundamental plane $\Delta \log(M/L_B)$ plotted against residual from the color-magnitude relation ΔCMR, residual from the $H\beta - \sigma$ relation, distance from BCG and galaxy mass. Different symbols refer to different morphological types. Error bars for colors and angular distances are assumed to be smaller than the symbol sizes. For the early-type galaxies, the p-values for statistical significance from the Spearman rank order correlation test are printed in the lower right corners. In panels (g) and (h) the magnitude limit $I \approx 21.15$ at which serious incompleteness due to uncertainties in the σ measurements sets in, is indicated with the solid line.

The residuals from this relation (positive means stronger $H\beta$) are plotted against the FP residual in Figure 2.6(c) and Figure 2.6(d). Only for MS 2053–04 are the error bars small enough to draw robust conclusions. A correlation is present, with confidence level 95.8%. $H\beta$ absorption lines are stronger for younger stellar populations, and the correlation with $\Delta\log(M/L_B)$ could confirm that the scatter in the FP is not random noise, but determined by age variations among the galaxies.

2.5.3 Location in the cluster

Here we consider if the enhanced scatter reported in §2.4.1 is related to environment. Clusters of galaxies are not isolated systems, as infall of galaxies from the field occurs. FP studies of field early-type galaxies indicate that their stellar populations may be somewhat younger than those of their counterparts in clusters (van Dokkum et al. 2001; Treu et al. 2002; van de Ven, van Dokkum,& Franx 2003; Rusin et al. 2003; van Dokkum & Ellis 2003; Gebhardt et al. 2003). In the cluster CL1358+62 van Dokkum et al. (1998) reported evidence for disky galaxies to be systematically bluer and to show a larger scatter in the CMR at larger radii (with the sample ranging to ~ 1 Mpc). As earlier studies of both clusters (K97; vD98) were based on one pointing, the larger scatter we find could be explained if residuals from the FP increase with distance from the BCG. Therefore, we might expect to see a gradient in age and larger scatter around the FP going to a larger range in cluster radii. For both clusters our samples extend to roughly 1 Mpc from the BCG. Figure 2.6(e) and Figure 2.6(f) do not show a significant correlation.

2.5.4 Galaxy mass and selection effects

Finally we try to explain the range of FP residuals as a function of galaxy mass. The mass M in solar units of a galaxy is calculated as follows (see JFK96):

$$\log M = 2\log\sigma + \log r_e + 6.07 \tag{2.8}$$

Figure 2.6(g) and Figure 2.6(h) show the residual from the FP against $\log M$. Only if we were to include the 6 galaxies with $\sigma < 100$ km s^{-1}, the trend of lower mass galaxies to have lower M/L ratios than predicted by the FP with JFK96 coefficients is significant at the 95% level.

For a good understanding of Figure 2.6(g) and Figure 2.6(h), we need to take into account that our FP samples are magnitude-limited, and not mass-limited. The FP can be rewritten as

$$M/L \sim M^{0.28} r_e^{-0.07}. \tag{2.9}$$

In the following, we ignore the dependence on r_e. Hence the residual is given by

$$\Delta M/L = \frac{M_{obs}/L_{obs}}{(M/L)_{FP}} = \frac{M_{obs}^{0.72}}{L_{obs}}. \tag{2.10}$$

For a fixed luminosity we expect all galaxies to fall on a line in a plot of $\Delta\log M/L$ versus $\log M$. In Figure 2.6(g) and Figure 2.6(h) this line is drawn for I=21.15. At this

magnitude serious incompleteness due to uncertainties in the σ measurements sets in. The lowest mass galaxies in Figure 2.6(a) and Figure 2.6(b) lie close to the line representing the magnitude limit. Low mass galaxies that lie on or above the FP would be too faint to allow for accurate dispersion measurements and would not enter the FP samples. Hence the few remaining low mass galaxies in our samples are brighter than their FP prediction based on r_e and σ.

Selection effects are clearly less relevant at the high mass end, and hence we determine the offset and scatter of the MS 2053–04 FP separately for the subsample of early-type galaxies with $M > 10^{11} M_\odot$ (following van Dokkum & Stanford 2003). For this subsample of 8 early-type galaxies we derive a zero-point shift with respect to Coma of $\Delta \log(M/L_B) = -0.288 \pm 0.056$ and a scatter of 0.132 ± 0.039 in $\log r_e$. As expected, this is slightly different from the zero-point shift of $\Delta \log(M/L_B) = -0.365 \pm 0.037$ for the full early-type sample. The zero-point offset is now in good agreement with K97, but the scatter is still larger.

If we apply a mass cut for the MS 1054–03 early-type galaxies of $M > 10^{11.5} M_\odot$, we find a shift in zero point of $\Delta \log(M/L_B) = -0.311 \pm 0.051$, compared to $\Delta \log(M/L_B) = -0.405 \pm 0.037$ for the full early-type sample. The scatter of the high-mass subsample (0.104 ± 0.030 in $\log r_e$) is similar to that of the full early-type sample (0.106 ± 0.023 in $\log r_e$).

2.5.5 Summary of correlations

We did not find evidence that FP residuals are related to environment. Instead, stellar population effects are playing a role in shaping the FP and selection effects in our magnitude-limited samples need to be taken into account.

First, early-type galaxies with stronger $H\beta$ absorption also tend to have lower M/L ratios than predicted by their r_e and σ. This correlation supports the interpretation of FP scatter as a measure of age variation among early-type galaxies. The larger FP scatter in MS 2053–04 therefore reflects a larger spread in relative ages than in the local universe. Comparison of FP residuals with residuals from the CMR cannot confirm or rule out the presence of such a stellar population effect.

Second, the fact that we do not see galaxies with low masses that lie on or above the FP, may be entirely explained by selection effects. Only low mass galaxies that are brightened by some recent star formation enter the FP sample. Their older counterparts are fainter than the magnitude limit for the dispersion measurements.

2.6 Evolution of M/L ratio

Correlations with residuals from the $H\beta - \sigma$ relation show that differences in FP zero point can be explained by age differences of the stellar population. In this section we study the evolution of the M/L ratio as a function of redshift and use this to estimate the mean formation redshift of cluster early-type galaxies. In Figure 2.7(a) we show the evolution of the M/L ratio with respect to Coma. Crosses refer to measured zero-point shifts from the literature: Coma at $z = 0.023$ (JFK96), CL1358+62 at $z = 0.33$ (K2000), CL0024+16 at $z = 0.39$ (van Dokkum,& Franx 1996), MS 2053–04 at $z = 0.583$ (K97),

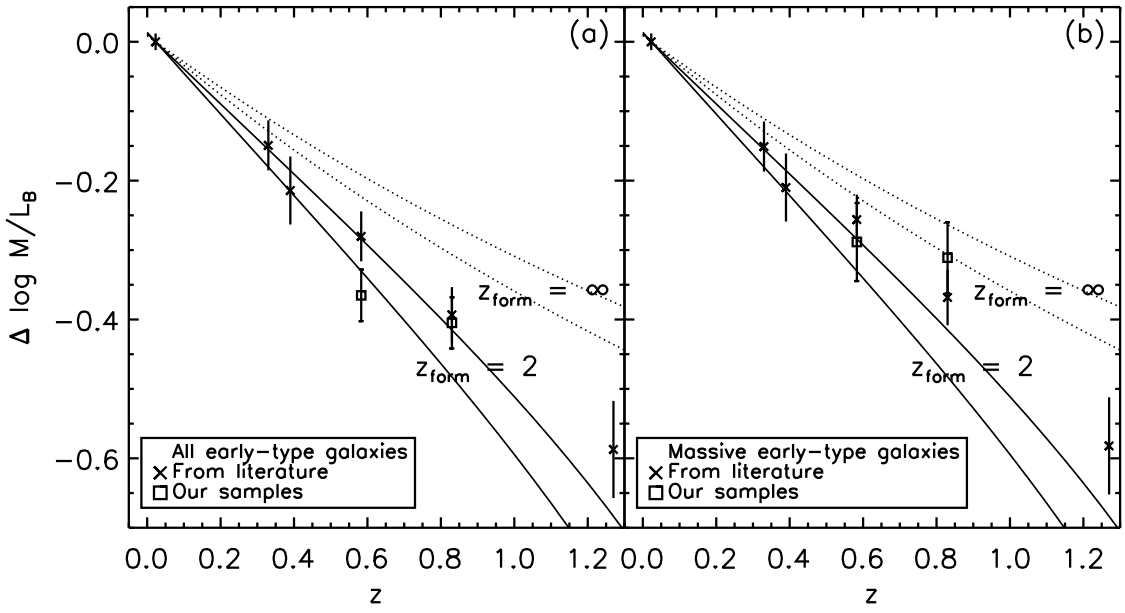

Figure 2.7 — Evolution of M/L with redshift. The cross symbols are results from the literature, namely Coma at $z = 0.023$ (JFK96), CL1358+62 at $z = 0.33$ (K2000), CL0024+16 at $z = 0.39$ (van Dokkum & Franx 1996), MS 2053–04 at $z = 0.583$ (K97), MS 1054–03 at $z = 0.83$ (vD98) and J0848+4453 at $z = 1.27$ (van Dokkum & Stanford 2003). Open squares denote the shift in M/L based on our larger samples for MS 2053–04 and MS 1054–03. Single burst models for $z_{form} = 2$ and ∞, assuming a Salpeter IMF ($x = 2.35$) and a range of metallicities, are drawn with solid and dotted curves, respectively. Panel (a) is based on all early-type galaxies, panel (b) shows results for the subsample of massive early-type galaxies ($M > 10^{11} M_\odot$ for clusters up to $z = 0.583$ and $M > 10^{11.5} M_\odot$ for the two higher redshift clusters).

MS 1054–03 at $z = 0.83$ (vD98) and J0848+4453 at $z = 1.27$ (van Dokkum,& Stanford 2003). The new results for MS 2053–04 and MS 1054–03, based on our larger samples, are plotted with open squares. Single burst evolutionary models for a formation redshift $z_{form} = 2$ and $z_{form} = \infty$ are drawn with a solid and dotted curve respectively. They represent a galaxy that is fixed in mass and whose luminosity evolves as:

$$L(t) \sim 1/(t - t_{form})^{\kappa} \tag{2.11}$$

Here t_{form} represents the age of the universe at the moment the stars were formed. κ depends on the slope of the IMF, passband and metallicity. For a Salpeter (1955) IMF and $-0.5 < [Fe/H] < 0.5$, the models of Bruzual & Charlot (2003), Vazdekis et al. (1996) and Worthey (1998) give $0.86 < \kappa_B < 1.00$. Using the new offsets for the two higher z clusters, the single burst model for a Salpeter IMF and solar metallicity favored by the least-squares method has $z_{form} \sim 2.26^{+0.28}_{-0.20}$. The 1σ confidence level was derived from the difference in χ^2 between the model and the overall minimum, $\Delta\chi^2 = \chi^2 - \chi^2_{min}$, to which Gaussian confidence levels were assigned (e.g., Press et al. 1992). As we showed in §2.5.4, the point of MS 2053–04 deviates from the earlier result (K97) since at low mass only galaxies with low M/L enter the magnitude-limited sample.

To avoid this bias, we apply a mass cut of $M > 10^{11} M_{\odot}$ to all clusters up to $z = 0.583$. A mass cut of $M > 10^{11.5} M_{\odot}$ was applied to MS 1054–03 and J0848+4453 since at these higher redshifts the selection effect sets in at a higher galaxy mass. For J0848+4453 two galaxies are left after omitting the one low mass outlier. As the biweight location estimator is robust against outliers, the zero-point shift only changes slightly for this cluster. We obtain the evolution of the M/L ratio as presented in Figure 2.7(b). Now the zero point of the MS 2053–04 FP follows the trend seen for the other clusters in Figure 2.7. If we constrain the analysis of the evolution in M/L ratio to massive early-type galaxies, a simple linear fit gives $\log M/L_B \sim -0.47z$, agreeing well with earlier determinations based on smaller samples or lower redshift (see, e.g., vD98). The formation redshift favored by a least-squares method is $z_{form} \sim 2.95^{+0.81}_{-0.46}$, slightly higher than the mean formation redshift for all early-type galaxies. A similar formation epoch for early-type galaxies in clusters was found by Kelson et al. (2001) based on the evolution of Balmer absorption-line strengths with redshift. It is remarkable how earlier studies of clusters based on smaller samples (see, e.g., K97; vD98) gave similar results.

2.7 Summary

We used visual and quantitative classifications to select bulge-dominated systems in our MS 2053–04 and MS 1054–03 samples. For MS 2053–04 we find a zero-point offset with respect to Coma of $\Delta \log(M/L_B) = -0.365 \pm 0.037$, larger than determined earlier on the basis of a smaller sample (K97). The scatter around the MS 2053–04 FP is 0.134 ± 0.034 in $\log r_e$, enhanced with respect to both K97 and the scatter in local clusters. The FP zero point of MS 1054–03 [$\Delta \log(M/L_B) = -0.405 \pm 0.037$] agrees well with the earlier result of $\Delta \log(M/L_B) = -0.393 \pm 0.040$ by vD98. The scatter of 0.106 ± 0.024 in MS 1054–03 is larger than reported by vD98 for a smaller sample of MS 1054–03 early-type galaxies. However, taking into account measurement uncertainties, the scatter is consistent with that in local clusters (JFK96). Late-type galaxies also follow the FP scaling relation and show a similar scatter around the FP as the early-type galaxies. Adding the late-type galaxies to the early-type sample results in a scatter of 0.136 ± 0.029 for MS 2053–04 and 0.117 ± 0.031 for MS 1054–03. The larger samples presented in this chapter allow us to study correlations with other properties of the early-type galaxies. We do not find evidence that the formation history depends on environment in the cluster. No significant correlation of FP residuals with CMR residuals was found. The presence of a correlation between FP residuals and residuals from the $H\beta - \sigma$ relation indicates that stellar population effects are playing a role. Assuming non-evolving slopes for all scaling relations, we find that galaxies with lower M/L than the FP prediction tend to show stronger $H\beta$ than predicted based on the $H\beta - \sigma$ relation. Finally, we show that the lack of low-mass galaxies on or above the FP may be entirely due to selection effects. To avoid a bias induced by the magnitude limit of our sample, we focus on the high-mass end, where selection effects are less relevant. Applying a mass cut at $M > 10^{11} M_{\odot}$ to all 4 considered clusters below $z \sim 0.6$ and at $M > 10^{11.5} M_{\odot}$ to the 2 higher redshift clusters at $z = 0.83$ and $z = 1.27$, increases the best fitting formation redshift from $z_{form} = 2.26^{+0.28}_{-0.20}$ to $z_{form} = 2.95^{+0.81}_{-0.46}$. The mass cut at $M = 10^{11} M_{\odot}$ is well below the typical mass of early-type galaxies: galaxies with

$M = 10^{11} M_{\odot}$ have dispersions of ~ 168 km s^{-1} which is significantly lower than the σ_* dispersion of early-type galaxies which is 228 ± 14 km s^{-1} (Kochanek 1994).
The implication of this work is that selection effects need to be taken into account, especially if the scatter is high. The scatter in MS 2053–04 is slightly higher than at low redshift; the scatter in the field at high redshift seems to be even higher (e.g., Gebhardt et al. 2003; van Dokkum & Ellis 2003). Hence, those studies are likely to suffer from much more significant selection effects.

Acknowledgments

We thank Arjen van der Wel for useful discussions on the fundamental plane. Based on data obtained at the W. M. Keck Observatory, which is operated as a scientific partnership among the California Institute of Technology, the University of California and the National Aeronautics and Space Administration. The Observatory was made possible by the generous financial support of the W. M. Keck Foundation. The authors wish to recognize and acknowledge the very significant cultural role and reverence that the summit of Mauna Kea has always had within the indigenous Hawaiian community. We are most fortunate to have the opportunity to conduct observations from this mountain.

References

Beers, T. C., Flynn, K.,& Gebhardt, K. 1990, AJ, 100, 32
Bender, R., Saglia, R. P., Ziegler, B., Belloni, P., Greggio, L., Hopp, U.,& Bruzual, G. 1998, ApJ, 493, 529
Bertin, E.,& Arnouts, S. 1996, A&AS, 117, 393
Bower, R. G., Lucey, J. R.,& Ellis, R. S. 1992b, MNRAS, 254, 589
Bruzual, G.,& Charlot, S. 2003, MNRAS, 344, 1000
Djorgovski, S.,& Davis, M. 1987, ApJ, 313, 59
Dressler, A., Lynden-Bell, D., Burstein, D., Davies, R. L., Faber, S.M., Terlevich, R. J.,& Wegner, G. 1987, ApJ, 313, 42
Fabricant, D., Franx, M.,& van Dokkum, P. G. 2000, ApJ, 539, 577
Gebhardt, K., et al. 2003, ApJ, in press
Hoekstra, H., Franx, M., Kuijken, K., van Dokkum, P. G. 2002, MNRAS, 333, 911
Jørgensen, I., Franx, M.,& Kjærgaard, P. 1995b, MNRAS, 276, 1341
Jørgensen, I., Franx, M.,& Kjærgaard, P. 1996, MNRAS, 280, 167 (JFK96)
Jørgensen, I. 1997, MNRAS, 288, 161
Jørgensen, I. 1999, MNRAS, 306, 607
Jørgensen, I., Franx, M., Hjorth, J.,& van Dokkum, P. G. 1999, MNRAS, 308, 833
Kelson, D. D., van Dokkum, P. G., Franx, M., Illingworth, G. D.,& Fabricant, D. 1997, ApJ, 478, L13 (K97)
Kelson, D. D., Illingworth, G. D., Franx, M.,& van Dokkum, P. G. 2000a, ApJ, 531, 137
Kelson, D. D., Illingworth, G. D., Franx, M.,& van Dokkum, P. G. 2000b, ApJ, 531, 159
Kelson, D. D., Illingworth, G. D., Franx, M.,& van Dokkum, P. G. 2000c, ApJ, 531, 184 (K2000)
Kelson, D. D., Illingworth, G. D., Franx, M.,& van Dokkum, P. G. 2001, ApJ, 552, L17
Kelson, D. D. 2003, PASP, 115, 688
Kelson, D. D., Illingworth, G. D., Franx, M.,& van Dokkum, P. G. 2006, ApJ, 653, 159
Kochanek, C. S. 1994, ApJ, 436, 56
Oke, J. B., et al. 1995, PASP, 107, 375
Press, W. H., Teukolsky, S. A., Vetterling, W. T.,& Flannery, B. P. 1992, Numerical Recipes. Cambridge Univ. Press, Cambridge
Rusin, D., et al. 2003, ApJ, 587, 143

Salpeter, E. 1955, ApJ, 121 161
Schlegel, D. J., Finkbeiner, D. P.,& Davis, M. 1998, ApJ, 500, 522
Trager, S. C., Worthey, G., Faber, S. M., Burstein, D.,& Gonzalez, J. J. 1998, ApJS, 116, 1
Tran, K. V., Kelson, D. D., van Dokkum, P. G., Franx, M., Illingworth, G. D.,& Magee, D. 1999, ApJ, 522, 39
Tran, K. V. 2002, PhD thesis, Univ. California at Santa Cruz
Tran, K. V., et al. 2003, submitted to ApJ
Treu, T., Stiavelli, M., Casertano, S., Møller, P.,& Bertin, G. 2002, ApJ, 564, L13
van de Ven, G., van Dokkum, P.G.,& Franx, M. 2003, MNRAS, 344, 924
van Dokkum, P. G.,& Franx, M. 1996, MNRAS, 281, 985
van Dokkum, P. G., Franx, M., Kelson, D. D., Illingworth, G. D., Fisher, D.,& Fabricant, D. 1998, ApJ, 500, 714
van Dokkum, P. G., Franx, M., Kelson, D. D.,& Illingworth, G. D. 1998, ApJ, 504, L17 (vD98)
van Dokkum, P. G., Franx, M., Fabricant, D., Illingworth, G. D.,& Kelson, D. D. 2000, ApJ, 541, 95
van Dokkum, P. G., Franx, M., Kelson, D. D.,& Illingworth, G. D. 2001, ApJ, 553, 39
van Dokkum, P. G.,& Stanford, S. A. 2003, ApJ, 585, 78
van Dokkum, P. G.,& Ellis, R.S. 2003, ApJ, 592, 53
Vazdekis, A., et al. 1996, ApJS, 106, 307
Worthey, G. 1998, PASP, 110, 888W